High-Throughput Continuous Hydrothermal Synthesis of Transparent Conducting Aluminium and Gallium Co-doped Zinc Oxides

Dougal P. Howard†, Peter Marchand†, Liam McCafferty†, Claire J. Carmalt†, Ivan P. Parkin† and Jawwad A. Darr†*

†Department of Chemistry, University College London, London WC1H 0AJ, United Kingdom

Keywords: continuous, hydrothermal, high-throughput, doped zinc oxides, conducting

ABSTRACT: High-throughput continuous hydrothermal flow synthesis was used to generate a library of aluminium and gallium co-doped zinc oxide nanoparticles of specific atomic ratios. Resistivities of the materials were determined by Hall Effect measurements on heat-treated pressed discs and the results collated into a resistivity-composition map. Optimal resistivities of ca. 9 x 10^{-3} Ω cm were reproducibly achieved for several samples e.g. co-doped ZnO with 2 at% Ga and 1 at% Al. The optimum sample on balance of performance and cost was deemed to be ZnO co-doped with 3 at% Al and 1 at% Ga.

Introduction

Synthesis of nano-scale (sub-100 nm diameter) particles has recently been of much interest in a number of different fields, intent on altering size, morphology, surface properties and functionality of otherwise known materials, optimizing properties for various applications.[1-5] For a highly efficient synthesis of nanoparticulate samples, High-Throughput Continuous Hydrothermal (HiTCH) flow synthesis approaches are attractive as sample libraries can be rapidly made. Continuous hydrothermal synthesis processes use aqueous metal salt solutions as precursors that are mixed with a flow of supercritical water to generate nanoceramic oxides in fractions of a second. Previously, the efficacy of such a synthesis approach was demonstrated in the synthesis of an entire ternary phase diagram of 66 samples in the Ce-Zr-Y oxide system in less than 12 h.[6,7] Similar arrangements were used in the synthesis of libraries of Eu-doped yttrium hydroxide phosphors,[8] Fe-doped lanthanum nickelates (fuel cell candidate cathodes)[9] and a rare-earth metal-doped zinc oxide photocatalysts.[10] The use of sustainable, high surface area and dispersed nanoparticles has also been shown to benefit a number of applications such as lithium-ion battery electrodes[11] and catalysts.[10] However in some applications, such as transparent conducting oxides (TCOs), the use of optimized and green nanoparticles is less well explored.

TCOs are a class of materials required to simultaneously possess high conductivity and high transmission of visible light in applications such as touchscreens,[12] solar cells,[13,14] smart windows,[15] organic light emitting diodes (OLEDS),[16] and flat panel displays.[17] Though often deposited as thin films by various sputtering methods from a solid target[18,19] or via chemical vapor deposition,[20] solution processing of TCO nanomaterials as high-solid content dispersions or inks offers an alternative to traditional methods.[21] These inks can be deposited by spin coating or ink-jet printing among other methods, which are cheaper and more sustainable processes than analogous sputtering techniques.[22-24] The high surface energy of the nanoparticles also allows the use of relatively low-temperature sintering techniques, suitable for deposition on temperature sensitive substrates. Towards this aim, nanoscaling of the particles can be useful, facilitating a homogeneous dispersion much more easily than with larger particles.

The most prevalent TCO material currently in use is indium tin oxide (ITO), which is used in > 90 % of current devices requiring transparent, conducting thin films.[25,26] However, increasing scarcity of indium has led to the drive to identify and develop alternative, inexpensive and sustainable materials. Among potential candidate materials are those based on doped titanium, tin, or zinc oxides.[27,28] These new materials have appropriate direct band gaps (> 3 eV) and have been used to generate thin films with optical transparencies > 80% and resistivities of the order of 10^{-4} Ω cm,[29-32] rivalling the properties of commercially available ITO.[25,26]

Doped zinc oxides are among the most studied ITO replacement materials, with particular promise being shown by aluminium-doping (i.e. aluminium-doped zinc oxide, AZO) and gallium-doping (i.e. gallium-doped zinc oxide, GZO).[33,34] Each of these dopants, however, have limitations. Aluminium-doping results in generally higher conductivities, but AZO is less chemically stable than GZO, potentially inhibiting processing techniques such as etching for the former.[35-37] Aluminium is also considerably cheaper than gallium and all of these factors must be taken into account. Co-doping of aluminium and gallium into

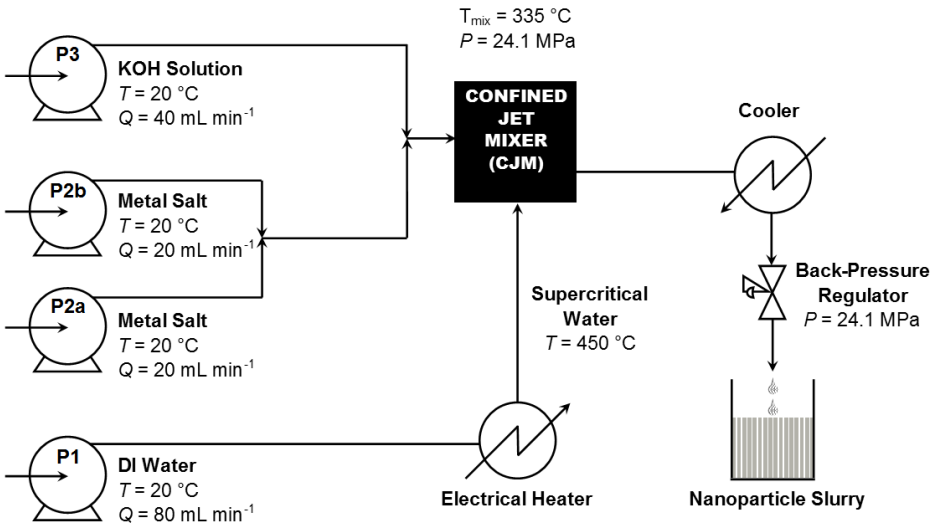

Figure 1. A schematic representing the continuous hydrothermal flow synthesis process described herein. 'T' represents temperature, 'Q' represents the flow rate for each pump, and 'P' represents pressure.

zinc oxide (AGZO), offers a balance of cost and performance (chemical stability and conductivity) with respect to AZO and GZO. The co-doping approach has yielded films with resistivities in the literature of ca. 10^{-4} Ω cm[38-43] and optical transparencies above 80 %[42-44] for thin films (deposited by magnetron sputtering). Whilst showing promise for TCO applications, AGZO has received relatively little attention in the literature compared to singularly doped AZO and GZO.

For the discovery of TCO nanomaterials with optimized dopant concentrations, the development of high-throughput synthesis (and faster or parallel screening) techniques is of importance for the speedy identification of new materials with optimal performance. High throughput combinatorial synthesis methods have been in use for over two decades.[45] The synthesis techniques have varied; they have included magnetron sputtering,[45-49] pulsed laser deposition,[50-52] molecular beam epitaxy,[53] flame pyrolysis,[54] sol-gel,[55] solid state,[56,57] and chemical vapor deposition,[58] and these have been used to synthesize materials with a variety of applications, including as superconductors,[45,50] TCOs,[45,47,51,59] photocatalysts,[53,55] and thermoelectrics.[56,57] These techniques are for the most part effective means towards the synthesis of combinatorial libraries in the form of thin films; with the exception of solid state[57] and spray pyrolysis[54] methods there has been a lack of combinatorial methodology for the direct production of metal oxide nanopowders. In addition to the applications abovementioned, the use of HiTCH flow synthesis has been previously shown to be an effective method for the high-throughput optimization of ITO nanomaterials with excellent electrical properties,[60] as well as singularly doped AZO and GZO.[61]

Herein, we report the synthesis of a library of 20 AGZO samples made via a HiTCH flow synthesis approach in less than 3 h, followed by processing and analysis of the materials to evaluate the properties of each sample in order to develop a conductivity map of the compositional space.

Experimental

Materials

Reagents were purchased from the following suppliers and used as-purchased; zinc nitrate hexahydrate, 98% (Sigma Aldrich, Dorset, UK), aluminium nitrate nonahydrate, 99+% (Sigma Aldrich, Dorset, UK), gallium nitrate hydrate, 99.99% (Alfa Aesar, Lancashire, UK), and potassium hydroxide (Fisher Scientific, Leicestershire, UK).

HiTCH flow synthesis of nanoparticles

Two pumps (Primeroyal K, Milton Roy, Pont Saint-Pierre, France) were used to provide the supercritical water and base feeds at 80 and 40 mL min^{-1}, respectively (pumps P1 and P3). The water used was 10 MΩ deionized water, purified using a Millipore Elix® Essential water purification system. The water feed from pump P1 was heated to 450 °C in flow using a 7 kW custom-built electrical water heater. The metal precursor feed was pumped by two Gilson 305 Pumps (pumps P2a and P2b), delivering a total flow rate 40 mL min^{-1}. The premixed precursor solutions consisted of the desired ratios of each zinc nitrate hexahydrate, aluminium nitrate nonahydrate and gallium nitrate hydrate, with a total metal concentration of 0.5 M. The metal precursor feed delivered from pumps P2a and P2b was first mixed with the 1.0 M KOH base feed in flow (from pump P3), before the combined mixture was introduced to a stream of supercritical water (from pump P1) in a patented Confined

Jet Mixer (CJM).[62] A schematic diagram of the reactor setup is shown in Figure 1. The reaction of the precursor solutions in the CJM resulted in the rapid crystallization of nanoparticles, with a theoretical mixing temperature of 335 °C, based on the flow rates and temperatures used.[63] The particle-containing aqueous combined flow was cooled to ca. 40 °C using a 1.5 m pipe-in-pipe heat exchanger, before passing through a back-pressure regulator (BPR). The nanoparticle slurries were collected in beakers and were then cleaned by repeated centrifugation and washing with deionized water until the decanted supernatant had conductivity below 50 μS as measured using a conductivity probe (model HI98311, Hanna Instruments, Leighton Buzzard, UK). The concentrated, clean slurry was then freeze-dried by slowly heating from -60 °C to 25 °C, under a vacuum of < 13 Pa, over 24 h using a Virtis Genesis 35XL freeze-drier.

Materials Characterization

Powder X-ray diffraction (XRD) data were collected using a STOE Stadi P diffractometer (Mo-Kα radiation, λ = 0.70932 Å) in transmission geometry. Data were collected in the 2θ range of 5 to 35 ° with a step size of 0.5 ° and a count time of 7 s step^{-1}. Scherrer analysis was carried out on the (100), (002), and (102) peaks, using a procedure that is detailed elsewhere.[64,65] Transmission electron microscopy (TEM) was carried out using a Jeol 200 kV transmission electron microscope in imaging mode. Powder samples were first dispersed in methanol (99.8 %) before being drop-coated onto carbon-coated copper TEM grids (Agar Scientific, Stansted, UK). Image and particle size analysis was carried out using ImageJ™ software. Further chemical analysis for Zn, Al, and Ga was performed by inductively coupled plasma atomic emission spectroscopy (ICP-AES) using dilute solutions of the samples dissolved in 1 vol% nitric acid. Analyses were carried out using a Varian 720 ICP-AES in axial configuration, equipped with an autosampler. Prior to sample analysis, calibration curves were established using standards at concentrations of 2.5, 5.0, 7.5 and 10.0 ppm for Zn and 0.25, 0.5, 0.75 and 1.0 ppm for Al and Ga, respectively. Raman spectra were collected with a Renshaw inViva Raman microscope, using a laser excitation at 514 nm; results are included in Figure S1 in the Supplementary Information. UV/vis/near-IR reflectance and transmittance spectra were taken using a PerkinElmer Precisely Lambda 950 spectrometer using an air background between 300 and 2500 nm.

To assess the conductivity of the materials, the powders were pressed into 16 mm diameter green-colored compacts of 1.0 mm thickness, under a force of 50 kN, using a Specac (Orpington, UK) bench-top hydraulic press. The discs were subsequently heat-treated at 500 °C for 3 h under a 5% H_2/N_2 atmosphere in a tube furnace (Elite Thermal Systems, Leicestershire, UK). Hall Effect measurements were carried out using an Ecopia HMS-3000 Hall Measurement System, and the bulk resistivity of the materials was obtained by use of the Van der Pauw method.[66] Four gold contacts were first sputtered onto each heat-treated disc, which was then subjected to an input current of 1 mA and a calibrated magnetic field of 0.58 T using the Van der Pauw probe. The transverse voltage was then measured, before the measurement was repeated by reversing the direction of the magnetic field and the current. Resistivity measurements were made in triplicate for each pellet and the mean value and standard deviations were calculated. A thin film was deposited by spin coating a 20 wt% dispersion of sample in water using a Laurell WS-650-23B spin coater at 2000 rpm.

Results and Discussion

Synthesis and Physical Characterization

The following naming convention was used in this work; each sample has been designated 'A_xG_yZO', such that x and y are the nominal at% of Al and Ga present in the precursor solution relative to the total concentration of metal ions. Thus, sample $A_{2.0}G_{1.0}ZO$ was synthesized with 2.0 at% Al, 1.0 at% Ga and 97.0 at% Zn in the precursor solution. Dopant proportions in the precursors were varied by 0.5 at%, with total dopant levels up to 5 at% (relative to 95 at% Zn). As-collected slurries were off-white/yellow, with color intensity increasing with an increase in dopant concentration. Ga was observed to have a greater impact on the color intensity than Al, consistent with other research conducted on the singularly doped AZO and GZO systems by the authors.[61] The yields of the products were consistently > 80 % by mass.

Detailed physical analysis was carried out on six representative samples across the compositional space, while electrical characterization was carried out on all samples. Physical and compositional characterization data is summarized in Table 1. Precise compositional analysis was carried out using ICP-AES. These results indicated that the level of dopant uptake was in the range 70 – 100 % of that expected on the basis of precursor concentrations (depending on the sample in question). The ICP data suggested that the doping levels of aluminium (rather than gallium) were generally closer to the values expected.

XRD patterns from the six representative samples are shown in Figure 2, with a standard reference pattern for ZnO.[67] All as-synthesized samples were phase-pure Wurtzite ZnO structure. The broad peaks of the XRD patterns were indicative of nano-crystallite samples; Scherrer peak analysis was carried out on the X-ray diffractograms for the (100), (002), and (101) peaks, the results for which are included in Table 1. Scherrer XRD crystallite size was observed to be consistent (within error) across all samples, in the range 16 to 17 nm, with a slight decrease in size with increasing total dopant level.

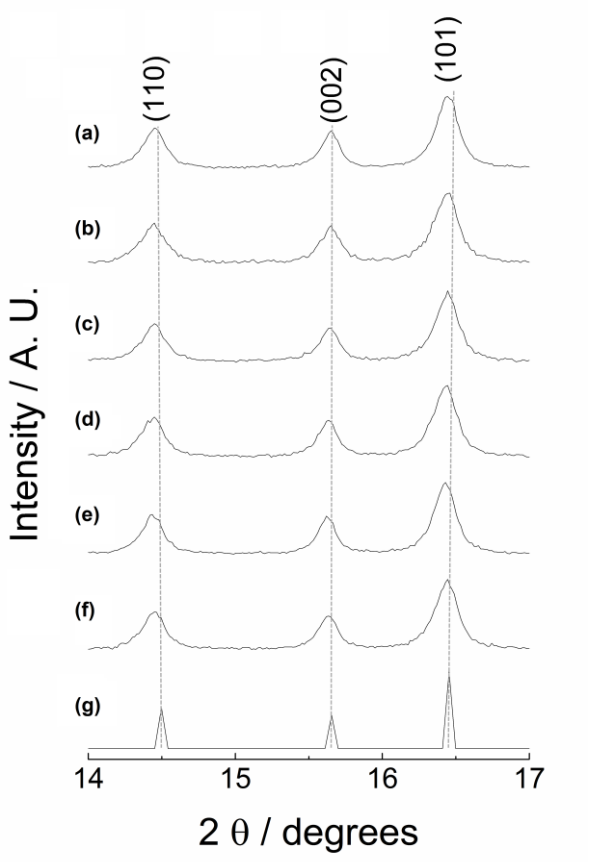

Figure 2. Powder XRD patterns of AGZO samples as-synthesized by continuous hydrothermal flow synthesis using Mo-Kα radiation (0.70932 Å). (a) $A_{3.0}G_{1.0}ZO$, (b) $A_{1.0}G_{3.0}ZO$, (c) $A_{2.0}G_{1.0}ZO$, (d) $A_{1.0}G_{2.0}ZO$, (e) $A_{1.5}G_{0.5}ZO$, (f) $A_{0.5}G_{1.5}ZO$, and (g) is a ZnO reference pattern (PDF No. 01-076-0704).[67] XRD data were collected using a Mo-Kα radiation, λ = 0.70932 Å, source.

TEM images revealed that the particle morphology across the compositional space investigated varied little, and was quantitatively consistent. Particle size analysis (carried out over 300 particles for each sample) showed that average particle size (within error) did not differ appreciably across the samples, with a size of 26.1 ± 13.5 nm at 2 at% total dopant level, to a size of 23.3 ± 10.0 nm at 4 at% dopant. The mean aspect ratio was 1.2 ± 0.3 for all samples analyzed. Representative TEM images of selected samples are shown in Figure 3. The particles were for the most part spheroidal, with some elongated to form short rods and a few, larger, 'arrowhead'-shaped nanoparticles. BET measurements showed a slight increase in surface area with increasing dopant level, consistent with the small decrease in primary particle size observed by TEM and XRD analysis, but all samples tested were in the range 25 to 30 $m^2 g^{-1}$. As the physical properties of the samples did not significantly vary across the range of samples investigated, it could be surmised that any effect on the electrical properties of the materials was predominantly due to the effect of their composition.

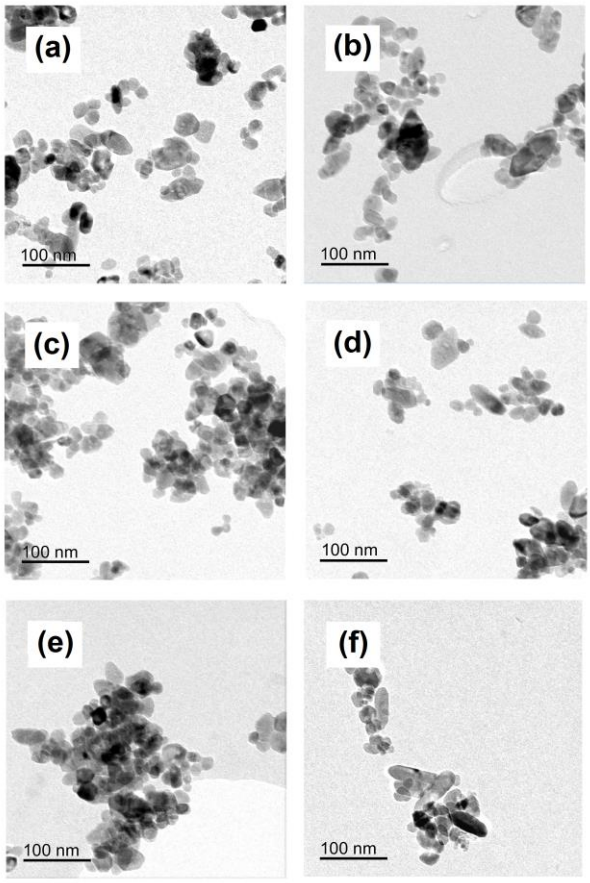

Figure 3. TEM images of AGZO samples: (a) $A_{0.5}G_{1.5}ZO$, (b) $A_{1.5}G_{0.5}ZO$, (c) $A_{1.0}G_{2.0}ZO$, (d) $A_{2.0}G_{1.0}ZO$, (e) $A_{1.0}G_{3.0}ZO$, and (f) $A_{3.0}G_{1.0}ZO$.

Electrical Characterization

Upon pressing of the powders into compacted discs, a color change was observed from yellow to green, with the intensity of the colors varying with the dopant levels in the samples. Heat-treatment in a reducing atmosphere resulted in further color change to blue. Values of the resistivities obtained are listed in Table S1 in the Supplementary Information, and visually depicted in Figure 4 in the form of a conductivity map, where red corresponds to the lowest conductivities and green corresponds to the highest. Included in the Figure are conductivity values obtained for the singularly doped AZO and GZO systems as reported previously,[61] giving the fullest possible view of the compositional space explored using this synthetic approach.

Table 1. Physical characterization data for six representative AGZO samples. Atomic percentage values were calculated from ICP-AES measurements, Scherrer crystallite size was calculated using the Scherrer equation[64,65] on the (110), (002), and (101) XRD diffraction peaks, and the mean particle length and aspect ratios were calculated for 300 particles for each sample from transmission electron micrographs.

Sample	Nominal Dopant Level / at%	Zn / at% (ICP-AES)	Al / at% (ICP-AES)	Ga / at% (ICP-AES)	Scherrer Crystallite Size / nm	Mean Particle Length / nm	Mean Aspect Ratio
$A_{0.5}G_{1.5}ZO$	2.0	98.4	0.5	1.1	17	26.3 ± 11.6	1.2 ± 0.3
$A_{1.5}G_{0.5}ZO$	2.0	98.6	1.1	0.3	17	26.1 ± 15.7	1.2 ± 0.3
$A_{1.0}G_{2.0}ZO$	3.0	97.8	0.8	1.3	17	26.1 ± 12.2	1.2 ± 0.3
$A_{2.0}G_{1.0}ZO$	3.0	97.9	1.4	0.7	17	25.0 ± 11.9	1.2 ± 0.3
$A_{1.0}G_{3.0}ZO$	4.0	96.6	0.9	2.5	16	23.2 ± 10.4	1.2 ± 0.3
$A_{3.0}G_{1.0}ZO$	4.0	96.9	2.3	0.8	16	23.4 ± 9.7	1.2 ± 0.3

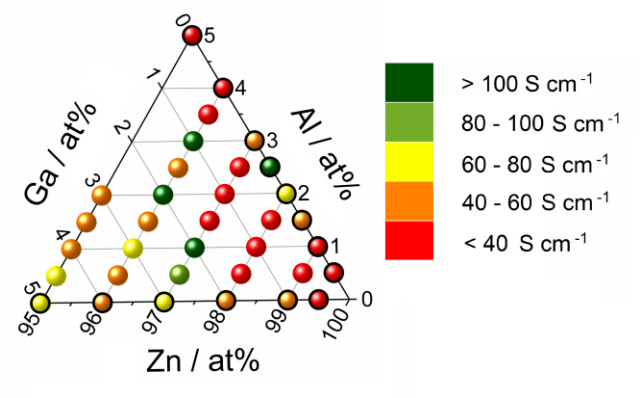

Figure 4. Conductivity 'map' describing the varying conductivity across the AGZO compositional space explored. At% of Zn is shown along the horizontal axis, Al at% increasing up the right-hand axis and Ga at% increasing down the left-hand axis, such that the bottom-right apex represents 100 at% Zn, the top apex represents 5 at% Al and 95 at% Zn, and the bottom-left apex represents 5 at% Ga and 95 at% Zn. Red coloration corresponds to low conductivity, while green coloration corresponds to higher conductivities. Points along the lower and right-hand axes (black encircled) are data points taken from previously published research into singularly-doped AZO and GZO nanomaterials, synthesized in like manner, included to contextualize the conductivities of the co-doped samples.[61]

While the majority of the compositional space displayed resistivities in the range 2 to 5 x 10^{-2} Ω cm, three compositions gave resistivities below 1.0 x 10^{-2} Ω cm (i.e. conductivities above 100 S cm^{-1}); these were $A_{3.0}G_{1.0}ZO$ at 9.4 x 10^{-3} Ω cm, $A_{2.0}G_{2.0}ZO$ at 9.3 x 10^{-3} Ω cm, and $A_{1.0}G_{2.0}ZO$ at 9.1 x 10^{-3} Ω cm. These compositions demonstrated electrical properties matching those found for optimal GZO samples synthesized and tested by the same methods, offering reduced cost compared to GZO samples (due to the introduction of aluminium to partially replace the gallium present in the structure). These values are almost an order of magnitude lower than the previously best reported resistivities of AGZO materials synthesized by CHFS-type processes.[68] The carrier concentrations in these highly conductive samples were 1.9 x 10^{19} cm^{-3}, 6.3 x 10^{18} cm^{-3}, and 6.5 x 10^{18} cm^{-3} for $A_{3.0}G_{1.0}ZO$, $A_{2.0}G_{2.0}ZO$, and $A_{1.0}G_{2.0}ZO$, respectively, while the carrier mobilities were 365 cm^2 V^{-1} s^{-1}, 139 cm^2 V^{-1} s^{-1}, and 122 cm^2 V^{-1} s^{-1}, respectively, showing considerably more variability than the resistivities. Thus, the composition of $A_{3.0}G_{1.0}ZO$ was found to be optimal with respect to electrical properties, showing both the highest measured mobility and charge carrier density. Whilst the charge carrier density was lower than that reported elsewhere by up to four times,[38,39,43,44] this can in turn rationalize the exceptionally high carrier mobility (10 times higher than that reported by the best performing AGZO materials)[38-44] in part due to reduced scattering effects from other charge carriers.

A 560 nm thin film of optimal material was deposited onto glass substrate by spin coating a 20 wt% dispersion in deionized water. After the same heat treatment as the discs previously, UV/vis/near-IR measurements were taken to gauge the transmission and reflectance of the film. These are shown in Figure 5. Transmission averaged 88 % over the visible range, well above industry requirements for such a film (which are typically 80 %).[12] The resistivity of the film was 1.5 (±0.5) x 10^{-2} Ω cm, the same order of magnitude as those measured for the analogous pressed discs of the same material.

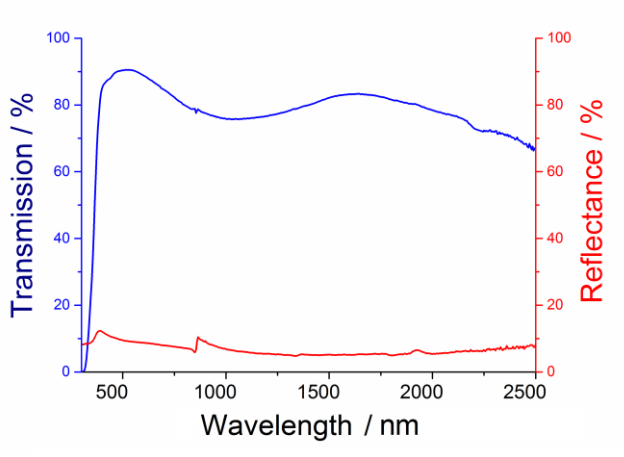

Figure 5. Transmission (blue) and reflectance (red) data for the spin coated film in the range 300 to 2500 nm, showing an average transmission of 88.4 % across the visible range. The artefact at 860 nm for both sets of data is due to the changeover from the tungsten to deuterium lamp in the spectrometer.

Conclusions

In summary, highly conductive AGZO materials were synthesized by high-throughput continuous hydrothermal flow synthesis, followed by heat-treatment of pressed compacts in a reducing atmosphere and testing by Hall Effect measurements. This was the first time such a compositional optimization had been carried for AGZO, and for any co-doped TCO material using a continuous hydrothermal synthesis method. Three regions in the compositional space explored were identified to have especially low resistivities of 9 x 10^{-3} Ω cm, and one in particular, synthesized with 3.0 at% Al and 1.0 at% Ga (with respect to 96.0 at% Zn) in the precursor solution, demonstrated an exceedingly high carrier mobility of 365 cm^2 V^{-1} s^{-1}, with carrier density of 1.9 x 10^{19} cm^{-1}. The promise of co-doping ZnO with both Al and Ga has been demonstrated by achieving electrical properties rivalling those of GZO, while reducing the relative cost of the material due to the partial use of Al as an inexpensive dopant. The applicability of the materials as conductive thin films was demonstrated by depositing optimal material onto a glass substrate; average transmission in the visible range was 88 %, with comparable resistivity to the pressed disc of the same powder.

ASSOCIATED CONTENT

Supporting Information. Table S1, a summary of the electrical data for each of the compositions of Al- and Ga-co-doped zinc oxide, and Figure S1, showing the Raman spectra for six representative samples across the compositional space.

AUTHOR INFORMATION

Corresponding Author

* Prof Jawwad A. Darr, e-mail: j.a.darr@ucl.ac.uk, telephone: +44 (0)20 7679 4345, address: Department of Chemistry, University College London, 20 Gordon Street, London, WC1H 0AJ

Author Contributions

All authors have given approval to the final version of the manuscript.

Funding Sources

The EPSRC is thanked for funding Award 1480036 (DPH), and the project with grant number EP/L017709/1 (JAD, CJC, IPP, PM).

ACKNOWLEDGEMENT S

Prof. John McArthur is thanked for technical support with ICP measurements.

ABBREVIATIONS

AGZO, aluminium and gallium co-doped zinc oxide; AZO, aluminium-doped zinc oxide; CJM, confined jet mixer; GZO, gallium-doped zinc oxide; HiTCH, high throughput continuous hydrothermal; ITO, indium tin oxide; TCO, transparent conducting oxide.

REFERENCES

1. Bogdan, J.; Zarzyńska, J.; Pławińska-Czarnak, J. Chances and limitations of nanosized titanium dioxide practical application in view of its physicochemical properties. *Nanoscale Res. Lett.* **2015**, *10*, 39
2. Zhao, Z.; Tian, J.; Sang, Y.; Cabot, A.; Liu, H. Structure, synthesis, and applications of TiO_2 nanobelts. *Adv. Mater.* **2015**, *27*, 2557-2582
3. Banin, U.; Ben-Shahar, Y.; Vinokurov, K. Hybrid semiconductor-metal nanoparticles: from architecture to function. *Chem. Mater.* **2014**, *26* (1), 97-120
4. Ashuri, M.; He, Q.; Shaw, L. Silicon as a potential anode material for Li-ion batteries: where size, geometry and structure matter. *Nanoscale* **2016**, *8*, 74-103
5. Sirelkhatim, A.; Mahmud, S.; Seeni, A.; Haida, N.; Kaus, M.; Ann, C.; Khadijah, S.; Bakhori, M.; Hasan, H.; Mohamad, D. Review on zinc oxide nanoparticles: antibacterial activity and toxicity mechanism. *Nano-Micro Lett.* **2015**, *7* (3), 219-242
6. Weng, X.; Cockcroft, J. K.; Hyett, G.; Vickers, M.; Boldrin, P.; Tang, C.; Thompson, S. P.; Parker, J. E.; Knowles, J. C.; Rehman, I.; Parkin, I. P.; Evans, J. R. G.; Darr, J. A. High-

throughput continuous hydrothermal synthesis of an entire nanoceramic phase diagram. *J. Comb. Chem.* **2009**, *11*, 829-834
7. Quesada-Cabrera, R.; Weng, X.; Hyett, G.; Clark, R. J. H.; Wang, X. Z.; Darr, J. A. High-throughput continuous hydrothermal synthesis of nanomaterials (part II): unveiling the as-prepared $Ce_xZr_yY_zO_{2-\delta}$ phase diagram. *ACS Comb. Sci.* **2013**, *15*, 458-463
8. Lin, T.; Kellici, S.; Gong, K.; Thompson, K.; Evans, J. R.; Wang, X.; Darr, J. A. Rapid automated materials synthesis instrument: exploring the composition and heat-treatment of nanoprecursors toward low temperature red phosphors. *J. Comb. Chem.* **2010**, *12*, 383-392
9. Alexander, S. J.; Lin, T.; Brett, D. J.; Evans, J. R.; Cibin, G.; Dent, A., Sankar, G.; Darr, J. A. A combinatorial nanoprecursor route for direct solid state chemistry: discovery and electronic properties of new iron-doped lanthanum nickelates up to $La_4Ni_2FeO_{10-\delta}$. *Solid State Ionics*, **2012**, *225*, 176-181
10. Goodall, J. B. M.; Illsley, D.; Lines, R.; Makwana, N. M.; Darr, J. A. Structure-property-composition relationships in doped zinc oxides: enhanced photocatalytic activity with rare earth dopants. *ACS Comb. Sci.* **2015**, *17*, 100-112
11. Johnson, I. D.; Lübke, M.; Wu, O. Y.; Makwana, N. M.; Smales, G. J.; Islam, H. U.; Dedigama, R. Y.; Gruar, R. I.; Tighe, C. J.; Scanlon, D. O.; Corà, F.; Brett, D. J.; Shearing, P. R.; Darr, J. A. Pilot-scale continuous synthesis of a vanadium-doped LiFePO4/C nanocomposite high-rate cathodes for lithium-ion batteries. *J. Power Sources* **2016**, *302*, 410-418
12. Gordon, R. G. Criteria for choosing transparent conductors. *MRS Bull.* **2000**, *25*, 52-57
13. Calnan, S.; Tiwari, A. High mobility transparent conducting oxides for thin film solar cells. *Thin Solid Films* **2010**, *518*, 1839-1849
14. Chopra, K.; Major, S.; Pandya, D. Transparent conductors – a status review. *Thin Solid Films* **1983**, *102*, 1-46
15. Granqvist, C.; Azens, A.; Hjelm, A.; Kullman, L.; Niklasson, G.; Rönnow, D.; Mattson, M. S.; Veszelei, M.; Vaivars, G. Recent advances in electrochromics for smart windows applications. *Sol. Energy* **1998**, *63*, 199-216
16. Park, J.-W.; Lee, G.-H.; Kwon, Y. Y.; Park, K.-W.; Lee, J.; Jin, W.; Nah, Y.-C.; Kim, H. Enhancement in light extraction efficiency of organic light emitting diodes using double-layered transparent conducting oxide structure. *Org. Electron.* **2014**, *15*, 2178-2183
17. Minami, T. Transparent conducting oxide semiconductors for transparent electrodes. *Semicond. Sci. Technol.* **2005**, 20, S35
18. Sittinger, V.; Ruske, F.; Werner, W.; Jacobs, C.; Szyszka, B.; Christie, D. High power pulsed magnetron sputtering of transparent conducting oxides. *Thin Solid Films* **2008**, *516*, 5847-5859
19. Kurita, D.; Ohta, S.; Ohta. H.; Koumoto, K. Carrier generation and transport properties of heavily Nb-doped anatase TiO_2 epitaxial films at high temperatures. *J. Appl. Phys.* **2006**, *100*, 096105-1
20. Dixon, S. C.; Scanlon, D. O.; Carmalt, C. J.; Parkin, I. P. n-Type-doped transparent conducting binary oxides: an overview. *J. Mater. Chem. C* **2014**, *4*, 6946-6961
21. Bühler, G.; Thölmann, D.; Feldmann, C. One-pot synthesis of highly conductive indium tin oxide nanocrystals. *Adv. Mater.* **2007**, *19*, 2224-2227
22. Hwang, H.-S.; Jeong, B.-Y.; Moon, J.; Chun, S.-K.; Kim, J. Ink-jet printing of indium tin oxide (ITO) films for transparent conducting electrodes. *Mater. Sci. Eng., B* **2011**, *176*, 1128-1131
23. Street, R. A.; Wong, W.; Ready, S.; Chabinye, M.; Arias, A.; Limb, S.; Salleo, A.; Lujan, R. Jet printing flexible displays. *Mater. Today* **2006**, *9*, 32-37
24. Al-Dahoudi, N.; Aegerter, M. A. Wet-chemical processing of transparent and antiglare conducting ITO coating on plastic substrates. *J. Sol-Gel Sci. Technol.* **2003**, *26*, 693-697
25. Stadler, A. Transparent conducting oxides – an up-to-date review. *Materials* **2012**, *5*, 661-683
26. Edwards, P. P.; Porch, A.; Jones, M. O.; Morgan, D. V.; Perks, R. M. Basic materials physics of transparent conducting oxides. *Dalton Trans.* **2004**, *17*, 2995-3002
27. An, H.-R.; Kim, C.; Oh, S.-T.; Ahn, H.-J. Effect of sol-layers on Sb-doped SnO_2 thin films as solution-based transparent conductive oxides. *Ceram. Int.* **2014**, *40*, 385-391
28. Bhachu, D. S.; Sathasivam, S.; Sankar, G.; Scanlon, D. O.; Cibin, G.; Carmalt, C. J.; Parkin I. P,; Watson, G. W.; Bawaked, S. M.; Obaid, A. Y.; Al-Thabaiti, S.; Bahasel, S. N. Solution processing route to multifunctional titania thin films: highly conductive and photocatalytically active Nb:TiO_2. *Adv. Funct. Mater.* **2014**, *24*, 5075-5085
29. Isherwood, P. J. M.; Neves, N.; Bowers, J. W.; Newbatt, P.; Walls, J. M. High quality aluminium doped zinc oxide target synthesis from nanoparticulate powder and characterization of sputtered thin films. *Thin Solid Films* **2014**, *566*, 108-114
30. Nam, E.; Kang, Y.-H.; Jung, D.; Kim, Y. S. Anode material properties of Ga-doped ZnO thin films by pulsed DC magnetron sputtering method for organic light emitting diodes. *Thin Solid Films* **2010**, *518* (22), 6245-6248
31. Nakao, S.; Yamada, N.; Hitosugi, T.; Hirose, Y.; Shimada, T.; Hasegawa, T. Properties of TiO_2-based transparent conducting oxides. *Thin Solid Films* **2010**, *518*, 3093
32. Yamada, N.; Hitosugi, T.; Kasai, J.; Hoang, N. L. H.; Nakao, S.; Hirose, Y.; Hasegawa, T. Transparent conducting Nb-doped anatase TiO_2 (TNO) thin films sputtered from various oxide targets. *Thin Solid Films* **2010**, *518* (11), 3101-3104
33. Ayadi, Z. B.; El Mir, L.; Djessas, K.; Alaya, S. The properties of aluminium-doped zinc oxide thin films prepared by rf-magnetron sputtering from nanopowder targets. *Mater. Sci. Eng. C* **2008**, *28*, 613-617
34. An, H.-R.; Ahn, H.-J.; Park, J. W. High-quality, conductive, and transparent Ga-doped ZnO films grown by atmospheric-pressure chemical-vapor deposition. *Ceram. Int.* **2015**, *41* (2), 2253-2259
35. Kumar, S.; Sarkar, B. Temperature-humidity tests and electrical analysis for the assessment of sheet resistance and power loss in photovoltaic cells. *International Journal of Current Engineering and Technology* **2013**, 3 (1), 123-128
36. Chang, Z. C. The effect of aging of ZnO, AZO, and GZO films on the microstructure and photoelectric property. *International Journal of Chemical, Molecular, Nuclear, Materials and Metallurgical Engineering* **2015**, 9 (6), 725-730
37. Chang, Z. C.; Liang, S. C. The microstructure of aging ZnO, AZO, and GZO films. *International Journal of Chemical, Molecular, Nuclear, Materials and Metallurgical Engineering* **2014**, 8 (5), 451-453
38. Son, Y. H.; Choi, S. H.; Park, J. J.; Jung, M. H.; Hur, Y.; Kim, I. S. Fabrication and study of transparent conductive films ZnO(Al) and ZnO(AlGa) by DC magnetron sputtering. *Journal of the Korean Vacuum Society* **2013**, *22* (3), 119-125
39. Kang, J.-H.; Lee, M.-H.; Kim, D. W.; Lim, Y. S.; Seo, W.-S.; Choi, H.-J. The annealing effect on damp heat stability of AGZO thin films prepared by DC moving magnetron sputtering. *Current Applied Physics* **2011**, *11* (3), S333-336
40. Kim, T. H.; Ju, Y.-G.; Park, L. S.; Lee, S. H.; Baek, J. H.; Yu, Y. M. Enhanced optical output power of tunnel junction

GaN-based light emitting diodes with transparent conducting Al and Ga-codoped ZnO thin films. *Jpn. J. Appl. Phys.* **2010**, *49* (9R), 091002
41. Zhu, K.; Yang, Y.; Song, W. Effects of substrate temperature on the structural, morphological, electrical and optical properties of Al and Ga co-doped ZnO thin films grown by DC magnetron sputtering. *Mater. Lett.*, **2015**, *145*, 279-282
42. Chang, S.-C. Post-annealed gallium and aluminium co-doped zinc oxide films applied in organic photovoltaic devices. *Nanoscale Res. Lett.* **2014**, *9* (1), 562
43. Liu, J.; Zhang, W.; Song, D.; Ma, Q.; Zhang, L.; Zhang, H.; Song, H. *Ceram. Int.* **2014**, *40* (8), 12905-12915
44. Seo, K.-W.; Shin, H.-S.; Lee, J.-H.; Chung, K.-B.; Kim, H.-K. *Vacuum* **2014**, *101*, 250-256
45. Xiang, X.-D.; Sun, X.; Briceno, G.; Lou, Y.; Wang, K.-A.; Chang, H.; Wallace-Freedman, W. G.; Chen, S.-W.; Schultz, P. G. A Combinatorial Approach to Materials Discovery. *Science* **1995**, *268*, 1738-1740
46. Perkins, J. D.; del Cueto, J. A.; Alleman, J. L.; Warmsingh, C.; Keyes, B. M.; Gedvilas, L. M.; Parilla, P. A.; To, B.; Readey, D. W.; Ginley, D. S. Combinatorial studies of Zn-Al-O and Zn-Sn-O transparent conducting oxide thin films. *Thin Solid Films* **2002**, *411*, 152-160
47. Perkins, J. D.; del Cueto, J. A.; Alleman, J. L.; Warmsingh, C.; Keyes, B. M.; Gedvilas, L. M.; Parilla, P. A.; Li. X.; To, B.; Readey, D. W.; Van Hest, M.; Ginley, D. S. Discovery and optimization of In-Sn-O based transparent conductors by combinatorial and pulsed laser deposition approaches. *Conference Record of the 29th IEEE Photovoltaic Specialists Conference, 2002* **2002**, 1126-1129
48. Taylor, M. P.; Readey, D. W.; Teplin, C. W.; van Hest, M.; Alleman, J. L.; Dabney, M. S.; Gedvilas, L. M.; Keyes, B. M.; To, B.; Parilla, P. A.; Perkins, J. D.; Ginley, D. S. Combinatorial Growth and Analysis of the Transparent Conducting Oxide ZnO/In (IZO). *Macromol. Rapid Comm.* **2004**, *25*, 344-347
49. Mao, S. S.; Burrows, P. E. Combinatorial screening of thin film materials: An overview. *Journal of Materiomics* **2015**, *1*, 85-91
50. Murakami, M.; Matsumoto, Y.; Nagano, M.; Hasegawa, T.; Kawasaki, M.; Koinuma, H. Combinatorial fabrication and characterization of ferromagnetic Ti-Co-O system. *Appl. Surf. Sci.* **2004**, *223*, 245-248
51. Perkins, J. D.; Taylor, M. P.; van Hest, M.; Teplin, C. W.; Alleman, J. l.; Dabney, M. S.; Gedvillas, L. M.; Keyes, B. M.; To, B.; Readey, D. W.; Delahoy, A. E.; Guo, S.; Ginley, D. S. Combinatorial optimization of transparent conducting oxides (TCOs) for PV. *Conference Record of the 31st IEEE Photovoltaic Specialists Conference, 2005* **2005**, 145-147
52. Watanabe, M.; Kita, T.; Fukumura, T.; Ohtomo, A.; Ueno, K.; Kawasaki, M. Combinatorial synthesis and high throughput evaluation of thermoelectric power factor in Mg-Si-Ge ternary compounds. *Appl. Surf. Sci.* **2007**, *254*, 777-780
53. Nakayama, A.; Suzuki, E.; Ohmori, T. Development of high throughput evaluation for photocatalyst thin-film. *Appl. Surf. Sci.* **2002**, *189*, 260-264
54. Kim, M.; Lai, S.; Laine, R. M. Combinatorial Nanopowder Synthesis Along the ZnO-Al_2O_3 Tie Line Using Liquid-Feed Flame Spray Pyrolysis. *J. Am. Ceram. Soc.* **2011**, *94*, 3308-3318
55. Henderson, S. J.; Armstrong, J. A.; Hector, A. L.; Weller, M. T. High-throughput methods to optically functional oxide and oxide-nitride materials. *J. Mater. Chem.* **2005**, *15*, 1528-1536
56. Funahashi, R.; Urata, S.; Kitawaki, M. Exploration of n-type oxides by high throughput screening. *Appl. Surf. Sci.* **2002**, *223*, 44-48
57. Wang, W.; Wang, J. Development of MnZn ferrites by combinatorial synthesis and high throughput screening method. *J. Alloys Compd.* **2008**, *463*, 112-118
58. Chadwick, N. P.; Glover, E. N. K.; Sathasivam, S.; Basahel, S. N.; Althabaiti, S. A.; Alyoubi, A. O.; Parkin, I. P.; Carmalt, C. J. Photo-activity and low resistivity in N/Nb Co-doped TiO_2 thin films by combinatorial AACVD. *J. Mater. Chem. A* **2016**, *4*, 407-415
59. Perkins, J. D.; Teplin, C. W.; van Hest, M.; Alleman, J. L.; Li, X.; Dabney, M. S.; Keyes, B. M.; Gedvilas, L. M.; Ginley, D. S.; Lin, Y.; Lu, Y. Optical analysis of thin film combinatorial libraries. *Appl. Surf. Sci.* **2004**, *223*, 124-132
60. Marchand, P.; Makwana, N. M.; Tighe, C. J.; Gruar, R. I.; Parkin, I. P.; Carmalt, C. J.; Darr, J. A. High-throughput synthesis, screening, and scale-up of optimized conducting indium tin oxides. *ACS Comb. Sci.* **2016**, *18*, 130-137
61. Howard, D. P.; Marchand, P.; Johnson, I. D.; Carmalt, C. J.; Parkin, I. P.; Darr, J. A. Conducting Al and Ga-doped zinc oxides; rapid optimization and scale-up. *J. Mater. Chem. A* **2016**, *4*, 12774-12780
62. Darr, J. A.; Tighe, C. J.; Gruar, R. I.; Co-current mixer, apparatus, reactor and method for precipitating nanoparticles. U.S. Patent 9,192,901, Nov 24, **2015**
63. Wagner, W.; Pruß, A. The IAPWS formulation 1995 for the thermodynamic properties of ordinary water substance for general and scientific use. *Journal of Physical and Chemical Reference Data* **2002**, 31, 387-535
64. Scherrer, P. Bestimmung der größe und der inneren struktur von kolloidteilchen mittels Röntgenstrahlen. *Nachr. Ges. Wiss. Goettingen, Math.-Phys. Kl.* **1918**, 98-100
65. Patterson, A. The Scherrer Formula for X-ray particle size determination. *Phys. Rev.* **1939**, *56* (10), 978-982
66. van der Pauw, L. J. A method of measuring specific resistivity and hall effect of discs of arbitrary shape. *Philips Res. Rep.* **1958**, *13*, 1-9
67. Schulz, H.; Thiemann, K. Structure parameters and polarity of the wurtzite type compounds SiC-2H and ZnO. *Solid State Commun.* **1979**, *32*, 783-785
68. Howard, D. P.; Marchand, P.; Gordon, T.; Darr, J. A. Sustainable transparent conducting oxide nanomaterials; aluminium- and gallium-co-coped zinc oxide (AGZO). *J. Nanosci. Nanotechnol.* **2016,** *16*, 10166-10171